

# Angular Vertical Comb-Driven Tunable Capacitor With High-Tuning Capabilities

Hung D. Nguyen, *Student Member, IEEE*, Dooyoung Hah, Pamela R. Patterson, *Member, IEEE*, Rumin Chao, Wibool Piyawattanametha, Erwin K. Lau, and Ming C. Wu, *Fellow, IEEE*

**Abstract**—This paper reports on a novel tunable capacitor with electrostatic angular vertical comb-drive (AVC) actuators. The AVC tunable capacitor creates a large offset in comb fingers through a small rotation angle—an advantage not found in conventional lateral comb-drive devices. High capacitance and large continuous tuning ratio is achieved in a compact device area. The largest tuning varactor demonstrates capacitance values between 0.27–8.6 pF—a tuning ratio of more than 31:1, the highest ever reported. The maximum quality factor  $Q$  is 273 at 1 GHz near the minimum capacitance value. [1012]

**Index Terms**—Angular vertical comb drive (AVC), BCB reflow, radio frequency microelectromechanical systems (RF MEMS), tunable capacitors.

## I. INTRODUCTION

IN RECENT years, microelectromechanical systems (MEMS) has become an emerging technology for radio frequency (RF) and wireless communications. In particular, MEMS varactors are very attractive for microwave and wireless circuits as phase shifters, tunable filters and voltage-controlled oscillators because of their large tuning range, high-quality factor  $Q$ , low-power consumption, and tolerance for high-voltage swings.

The capacitance of a MEMS varactor can be tuned by either moving the dielectric between the conductors [1], or changing the spacing between conductors or their overlapped area [2]–[5]. Several actuation mechanisms have been reported, including thermal [2], piezoelectric [3], or electrostatic actuation [4], [5]. Electrostatically driven varactors have received the most attention because of low power consumption, fast response time, and ease of control due hysteresis-free tuning. The simplest type of tunable capacitor called gap-closing actuator consists of a pair of parallel plate conductors whose spacing is varied by applying a dc voltage. Unfortunately, they exhibit highly nonlinear actuation and suffer from the pull-in phenomenon, which restricts the continuous tuning range to a 50% theoretical limit and confines these devices to digital tuning applications [6], [7].

There have been attempts to overcome this theoretical limit by using different gap spacings for the actuator and the capac-

itor, or using a push-pull geometry. Zou *et al.* [8] achieved a tuning range of 69% while Dec and Suyama [9] obtained an 87% change in capacitance with these approaches. However, these modifications demonstrate only moderate increases. Complete separation of the sensing and actuating electrodes has further increase the tuning performance to 400% [10] and 600% [11].

In recent years, lateral comb-drive actuators have shown to be a superior alternative to gap-closing actuators for tunable capacitors [12]. Lateral comb actuators suffer less from the pull-in phenomena and thus tuning is more easily controlled. Comb drive actuators have made it possible to achieve a tuning ratio from 8.4 to 1 with low operating voltages. However, a larger tuning range requires larger comb separation, which has the negative effect of increasing overall device size.

Previously, we propose a novel MEMS tunable capacitor with angular vertical comb-drive (AVC) actuators [13]. Unlike lateral comb-drives, a small out-of-plane rotation from the AVC results in a large offset between comb electrodes. The AVC also allows for continuous rotation without pull-in. Thus, a large continuous tuning range can be realized in a compact device.

In this paper, we report on the details of the AVC tunable capacitors. With an improved design, a continuous tuning range of nearly 3000% has been achieved. We believe this is the highest tuning range reported to date. This paper is organized as follows: in Section II, we describe the working principle and the modeling of the varactor. Section III continues with the details of the fabrication process. Section IV shows the experimental results before concluding.

## II. DESIGN PRINCIPLE

Fig. 1 shows the schematics of the AVC tunable capacitor at (a) zero bias (maximum capacitance) and at (b) maximum applied voltage (minimum capacitance). The tuning mechanism of the AVC varactor is similar to that of a conventional bulk variable capacitor as shown in Fig. 2, [14]. The varactor design uses two sets of interdigitated comb fingers located at opposite ends. The shorter comb fingers are the driving electrodes while the longer comb fingers serve as the sensing (RF) electrodes. Upon release and with no applied voltage, the suspended driving comb finger electrodes are batch-assembled to a prescribed angle above the ground plane. At the opposite end of the device, the suspended sensing comb fingers remain parallel with the fixed fingers. In this state, the capacitance is at a maximum due to the maximum overlapping area between the sensing electrodes. When actuated, the suspended driving comb fingers are rotated down towards the fixed fingers while the sensing fingers

Manuscript received March 3, 2003; revised September 6, 2003. This work was supported in part by HRL Laboratories under the University of California MICRO program, and by DARPA under Contract N66001-99-C-8635. Subject Editor D. Cho.

H. D. Nguyen, D. Hah, W. Piyawattanametha, E. K. Lau, and M. C. Wu are with the University of California, Los Angeles, CA 90095 USA (e-mail: hnguyen@icsl.ucla.edu).

P. R. Patterson is with HRL Laboratories, LLC, Malibu, CA 90265 USA.

R. Chao is now with National Cheng Kung University, Tainan 701, Taiwan.

Digital Object Identifier 10.1109/JMEMS.2004.828741

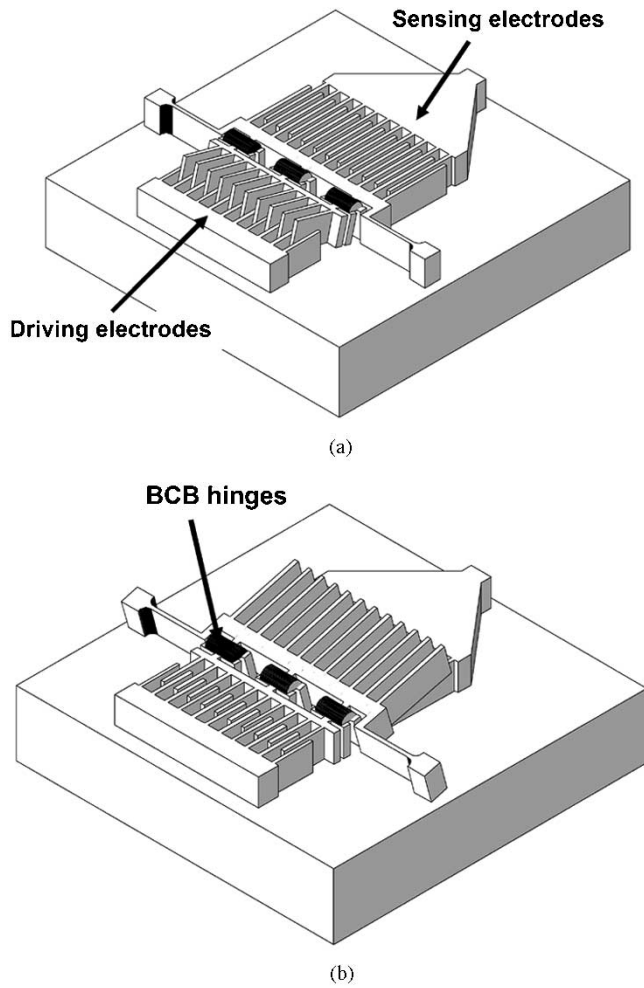


Fig. 1. Schematic of the AVC tunable capacitor at (a) maximum capacitance/zero bias and (b) minimum capacitance/maximum bias.

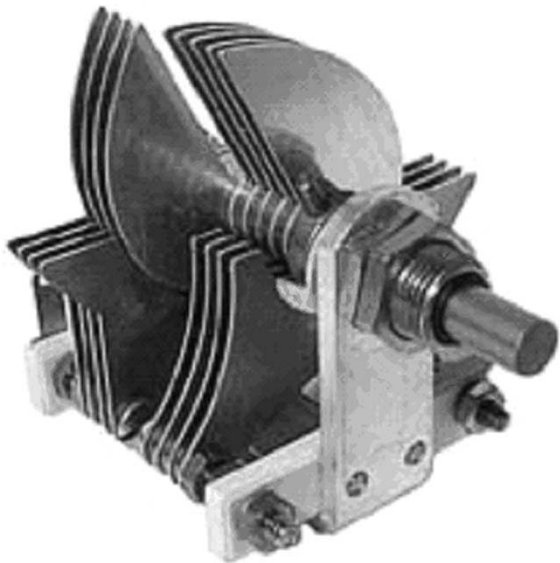


Fig. 2. Photograph of a conventional variable capacitor. Tuning the capacitance is achieved through the rotation of one set of metal blades to vary the overlapping area.

are lifted up from the substrate. The decrease in overlapping area between the sensing comb fingers reduces the capacitance.

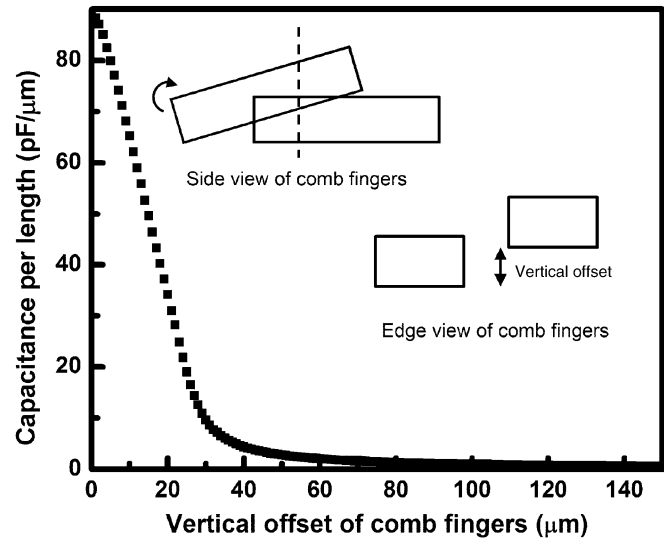


Fig. 3. The calculated capacitance per unit length versus vertical finger offset between a pair of comb fingers with a thickness of  $25 \mu\text{m}$  and a gap spacing of  $2.47 \mu\text{m}$ . The inset shows the cross section of the comb fingers with the vertical offset.

The AVC actuator, which we have previously implemented on a MEMS scanning mirror, offers large tilting angles at low voltages [15]. An analytical model of the electrostatic actuation was derived from a previous work by Hah *et al.* on staggered comb-drive actuators [16]. The derivation starts with the equilibrium equation between the electrostatic and mechanical torques

$$T_e(\theta) = \frac{V^2}{2} \frac{\partial C}{\partial \theta} = NV^2 \frac{\partial C_{\text{unit}}}{\partial \theta} \quad (1)$$

$$T_m(\theta) = k_s \theta \quad (2)$$

where  $V$  is the applied voltage,  $C$  is the capacitance between the electrodes,  $C_{\text{unit}}$  is the capacitance per finger length,  $N$  is the number of finger pairs, and  $k_s$  is the torsional spring constant. Following the derivation given by Hah, the pull-in condition is described by the expression

$$\text{PI}(\theta) = \frac{\partial C}{\partial \theta} - \theta \frac{\partial^2 C}{\partial \theta^2} > 0 \quad (3)$$

where (3) is written in terms of the change in  $C$  between the fixed and rotating finger electrodes with respect to the rotation angle  $\theta$ . To avoid pull-in, (3) must be greater than zero for all angles  $\theta$ . (3) can be rewritten in terms of physical finger dimensions to determine the appropriate configuration for the actuator.

While the analytical calculations provide a good approximation of the transfer curve and capacitance values, it does not take into account the capacitance from fringe fields. Instead, we use two-dimensional numerical analysis to attain a more accurate expression for the capacitance which we then use in (3). We first determine the unit capacitance of a finger cross section at various offsets between two fingers and then integrate over the entire length of the finger electrodes. The inset of Fig. 3 shows the moving finger at an angle above the fixed finger electrode. The figure also shows a cross section of the same fixed and moving fingers along the dashed line. We position one comb finger (right) with a vertical offset above the fixed finger (left).

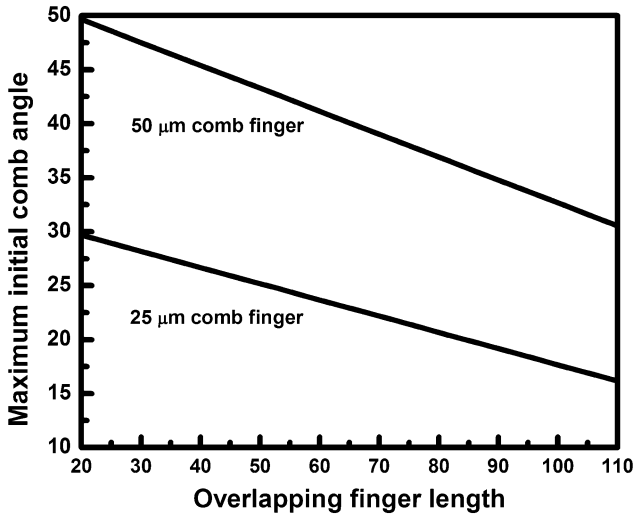


Fig. 4. The calculated maximum initial angle of the actuating comb without pull-in versus actuating comb finger length for 25- $\mu\text{m}$  and 50- $\mu\text{m}$ -thick fingers.

The calculation assumes a finger thickness and a gap spacing of 25  $\mu\text{m}$  and 2.47  $\mu\text{m}$ , respectively. Given the dimensions, the Matlab software determines the electric potential between the cross sections and calculates the unit capacitance for each offset position. These values are shown on the  $y$ -axis of Fig. 3 as a function of the vertical offset. Note that the capacitance is finite and not zero when the fingers are completely separated due to the contributions from fringe fields. The curve for the unit capacitance in Fig. 3 can be approximated by a Gaussian function using least square fit

$$C_{\text{unit}}(y) = C_1 + C_2 e^{-\left(\frac{y}{C_3}\right)^2}$$

$$C_1 = 5.25 \times 10^{-13} \quad C_2 = 1.57 \times 10^{-10}$$

$$C_3 = 3.56 \times 10^{-5}. \quad (4)$$

With (4) we can integrate to obtain the equation for the total capacitance between the rotating and static comb fingers

$$C(\theta) = \int_{l_{\text{offset}} \cos(\theta_{\text{initial}} - \theta)}^{l_{\text{finger}} \cos(\theta_{\text{initial}} - \theta)} \left( C_1 + C_2 e^{-\left(\frac{y}{C_3}\right)^2} \right) dy. \quad (5)$$

We can proceed to solve the pull-in condition and electrostatic torque. While a three-dimensional numerical analysis is more comprehensive, the hybrid analytical/two-dimensional numerical analysis has a much shorter computation time and can be used iteratively for optimization. For simplicity, we assume that the cross sectional areas of the fingers are constant regardless of the rotation angle. Furthermore, we neglect any unwanted lateral electrostatic forces especially at small angles. While we have observed some lateral motion at large voltages, this can be remedied by increasing the lateral spring constant through modifications to the shape of the torsion springs [17]. From the numerical analysis and (3) we can approximate the tuning capability of the AVC varactor and the appropriate finger dimensions. We determine that given an electrode length, there exist a maximum initial reflow angle such that pull-in can be avoided. Fig. 4 shows the maximum initial angle as a function of actuating comb finger length for two different comb finger thick-

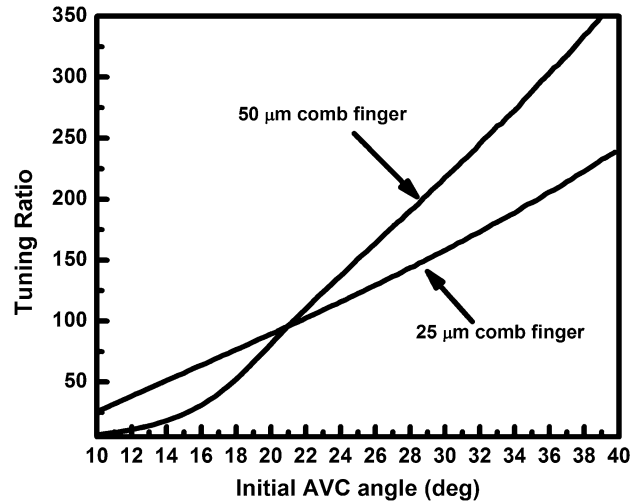


Fig. 5. Calculated tuning ratio versus the initial tilt angle for AVC tunable capacitors with 25- $\mu\text{m}$  and 50- $\mu\text{m}$ -thick comb fingers.

nesses: 25  $\mu\text{m}$  and 50  $\mu\text{m}$ . The figure shows that migration to thicker comb fingers (50  $\mu\text{m}$ ) allows for larger initial AVC angles without pull-in for the same comb finger length.

We have also found that wider tuning range can be obtained with thicker comb fingers. Thicker finger electrodes allow for larger rotation angles, which reduce the minimum capacitance and increases the maximum capacitance through a larger overlapping area. Fig. 5 shows the calculated tuning ratio for devices with 25- $\mu\text{m}$  and 50- $\mu\text{m}$ -thick fingers. Both curves are based on sensing comb finger length of 350  $\mu\text{m}$ . For small initial AVC angles, the thinner device has larger tuning ratio because the sensing fingers are completely separated in the minimum capacitance state but for large initial angles, the 50- $\mu\text{m}$ -thick device exhibits higher tuning ratio than the thinner devices. The actuation voltage also reduces with increasing finger thickness and lengths. The plot predicts tuning ratios greater than 100 for both device thicknesses however, it should be noted that the calculation assumes capacitance contribution from the finger electrodes only and not between the bonding pads and ground plane. The measured minimum capacitance will be larger due to this stray capacitance and therefore the maximum calculated tuning ratio is not attainable in practical devices.

### III. FABRICATION

Fig. 6 shows the details of the fabrication process. The tunable capacitor is fabricated on a glass substrate to reduce parasitic capacitance. The silicon-on-glass wafer is created by bonding a silicon-on-insulator (SOI) wafer to a Borofloat glass wafer. We chose Borofloat glass as the substrate because of the similar thermal expansion coefficient with that of silicon (3.25 ppm/ $^{\circ}\text{C}$ ) and the high etch rate in hydrofluoric (HF) acid. Prior to bonding, the SOI and the Borofloat glass wafers are thoroughly cleaned and dehydrated to ensure a hydrophilic surface between the wafers for complete contact. The wafers are then anodically bonded at 400  $^{\circ}\text{C}$  and 700 V [see Fig. 6(a)]. The SOI substrate is subsequently removed by a combination of mechanical and chemical etches [see Fig. 6(b)]. The exposed buried oxide is also etched in a buffered hydrofluoric etch (BOE) solution. The 25- $\mu\text{m}$ -thick silicon film is then patterned

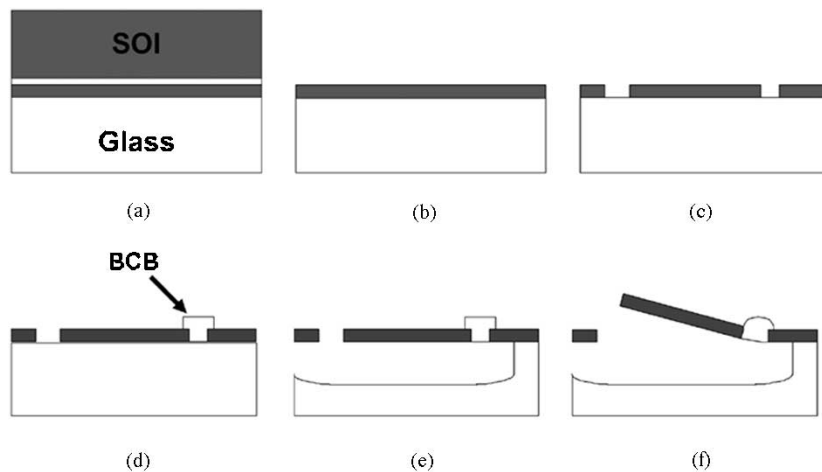


Fig. 6. Fabrication process flow for MEMS AVC tunable capacitor.

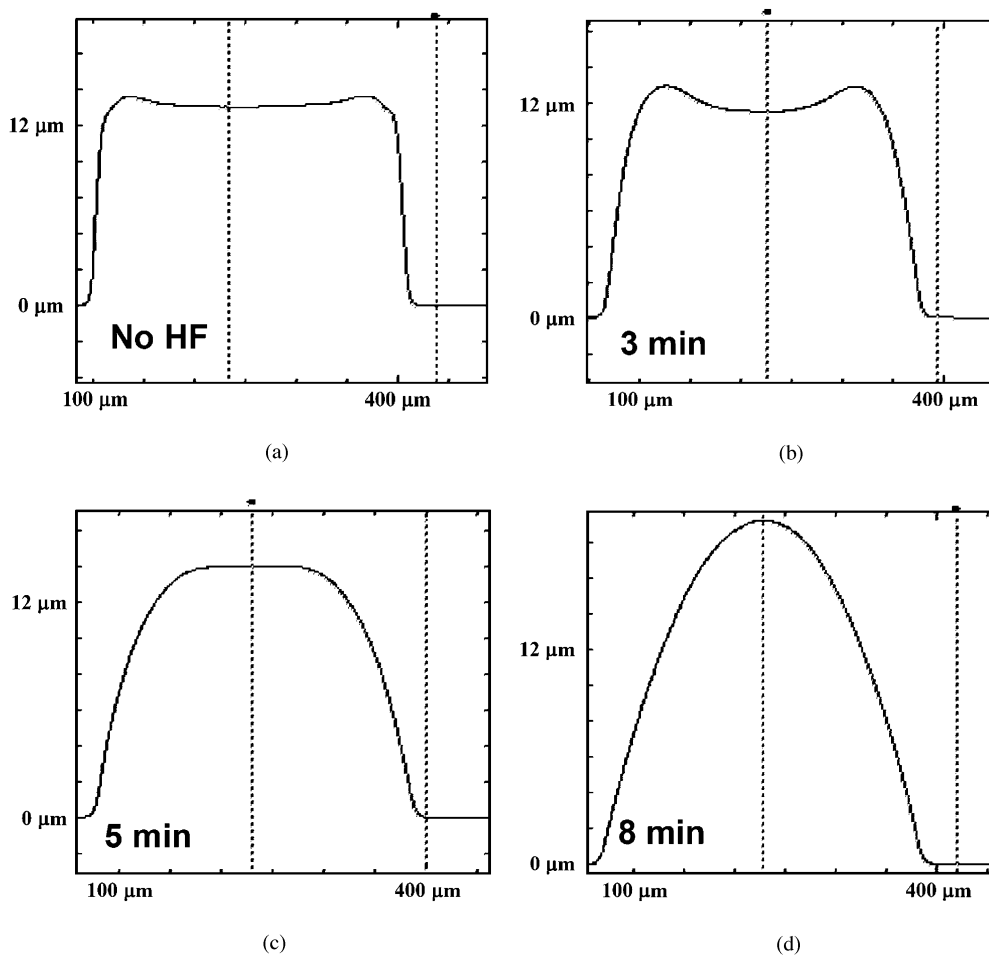


Fig. 7. Surface profiles of BCB test structures with various exposure times (0, 3, 5, and 8 min) to HF after reflow at 400°C for 20 min.

and deep reactive ion etched (DRIE) to form the device structure [see Fig. 6(c)]. Next, photosensitive Cyclotene resist (BCB) hinges are patterned to physically connect the two sets of suspended comb fingers [see Fig. 6(d)]. The BCB hinges are then cured at 300 °C to increase robustness for subsequent etching processes. The glass substrate is etched in 49% hydrofluoric acid for 10 min at an etch rate of 7 μm/min to ensure the complete undercutting and release of the suspended fingers [see Fig. 6(e)]. Supercritical drying is essential to minimize

release stiction, particularly between the long comb fingers. After supercritical drying, the hinges are recured at 400 °C in a nitrogen-overpressured oven for twenty minutes. The movable dc comb fingers are assembled to an initial angle above the substrate plane due to the surface tension of the reflowed hinges [see Fig. 6(f)]. The final process step involves the metallization over the entire sample with sputtered aluminum for better conductivity. The metallization electrically connects both the floating sensing and actuating fingers by covering over the

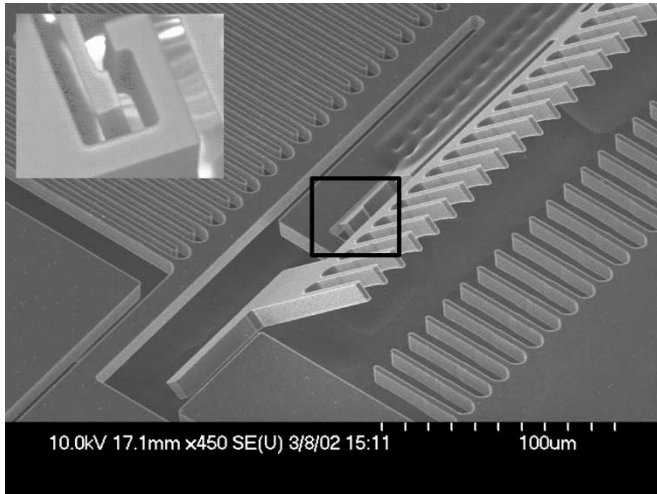


Fig. 8. SEM Micrograph of a 10- $\mu\text{m}$ -thick tunable capacitor at the maximum capacitance state. The top and bottom inset shows two different limiter designs.

BCB hinge. Both suspended finger electrodes are connected to the RF ground plane through the torsional beams. The fixed actuating fingers are electrically isolated from the rest by a DRIE trench.

The AVC comb fingers are batched assembled by surface tension of reflowed BCB. Batch self-assembly using surface tension of reflowed hinges have been reported. Reflow of metal solders [18]–[20] and photoresist [21] has shown to successfully assemble three-dimensional MEMS devices. BCB polymer is traditionally used in millimeter-wave integrated circuit (MMIC) technology for planarization or as a dielectric material, but it has never been used for self-assembly in MEMS fabrication. BCB polymers offer many important features that photoresist lacks. It is more resistant than photoresist toward acids and solvents that are commonly used in microfabrication. This allows us to release the devices in pure hydrofluoric acid without fear of degradation or delamination of the hinges. In fact, uncured BCB can withstand prolong exposure to HF without signs of deterioration in contrast to that of photoresist where delamination of the film in HF is well documented. Furthermore, since BCB is a negative resist, there is no problem with the removal of trapped BCB within the deep grooves of the etched silicon device layer.

Reflowed BCB microlenses have been reported [22], however, no detailed process was mentioned. We found that the reflow of BCB relies heavily on the exposure to HF. We have seen no evidence of reflow on test samples by curing BCB above its glass transition temperature. However, reflow is clearly evident when the resist comes in contact with HF even with fully cured BCB. Fig. 7 shows the effects of HF on various circular test structures with 300  $\mu\text{m}$  diameter and 12  $\mu\text{m}$  height. Without exposure to HF, the square profile of the cured BCB remains cylindrical [see Fig. 7(a)]. With increasing soaking time, the edges of BCB start to reflow [see Fig. 7(b) and (c)]. When BCB is soaked in HF for longer than 8 min, full reflow into a spherical shape was observed [see Fig. 7(d)].

During reflow, the surface tension pulls the suspended driving electrodes to its prescribed angle. This angle is determined by physical limiters that prevent further rotation above the designated angle. The suspended sensing comb fingers do not rotate

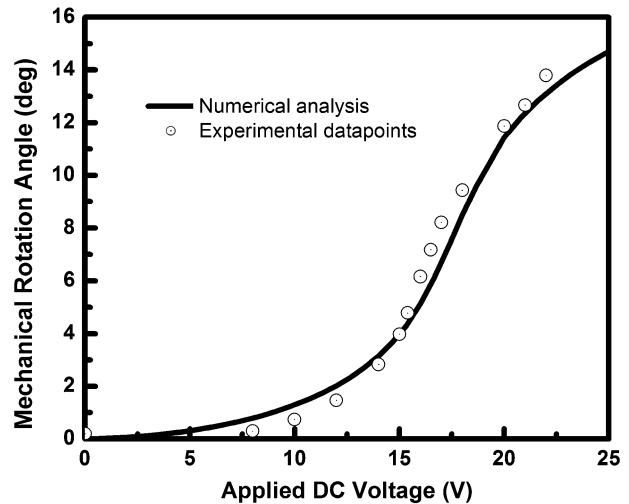


Fig. 9. Mechanical rotation angle of the RF sensing comb versus voltage for the 25- $\mu\text{m}$ -thick AVC tunable capacitor.

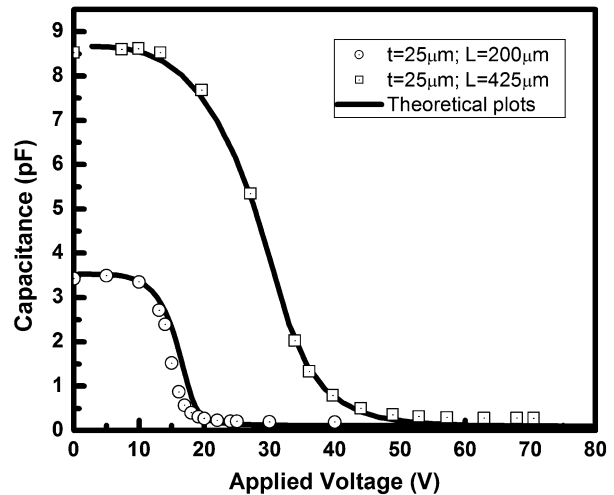


Fig. 10. Measured and calculated capacitance-versus-voltage curves for 25- $\mu\text{m}$ -thick AVC tunable capacitors with 200 and 425- $\mu\text{m}$ -long capacitance comb fingers.

out-of-plane because they are securely anchored at either side of the device by the torsion springs. A scanning electron micrograph (SEM) of the device, including the suspended fingers upon release and assembly, is shown in Fig. 8. The figure shows that the limiters do not catch. However, without the presence of the limiters, the BCB hinges can easily rotate our test devices a full 180°. Furthermore our limiters have a yield of 93% for reflow angles of  $20^\circ \pm 2^\circ$ . Thus, we conclude that these limiters do catch during the reflow process at 400 °C but as the device is cooled, the thermal contraction of the BCB hinge retracts the limiters away from the sidewalls. This does not affect the reflow angle since the fingers are already permanently fixed at the desired angle. Additional investigation of temperature effects on the BCB hinges is underway.

#### IV. EXPERIMENTAL RESULTS

Fig. 9 shows the theoretical and measured mechanical angle versus the applied voltage for the 25- $\mu\text{m}$  device layer. The actuating fingers are 70- $\mu\text{m}$  long with a width and gap spacing of

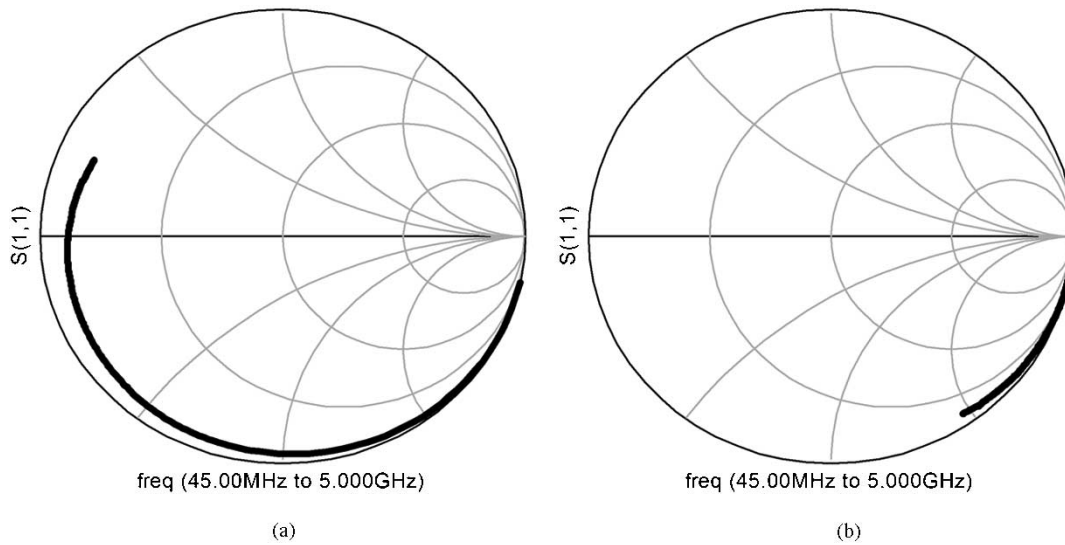


Fig. 11.  $S_{11}$  smith chart at (a) maximum capacitance and (b) minimum capacitance from 45 MHz to 5 GHz.

3  $\mu\text{m}$ . The initial reflow angle is set at  $20^\circ$ . The sensing electrodes share similar width and gap spacing but their length is 200  $\mu\text{m}$ . The restoring mechanical torque comes from a pair of 350- $\mu\text{m}$ -long rectangular torsion springs. These springs also have 4- $\mu\text{m}$  widths. For reasonable capacitance values and actuation voltage, the varactor has 100 pairs of sensing and actuating finger electrodes. Interferometric scans were used to obtain different rotation angles at different voltages. The curve represents the mechanical rotation angle of the sensing comb fingers. However, angles greater than the numerical aperture of the collecting optics ( $15^\circ$ ) are difficult to detect in our current experimental setup.

The capacitance and the  $S$  parameters are measured with an Agilent microwave network analyzer 8510C and a high-frequency coplanar waveguide probe with a ground-signal-ground configuration from GGB Industries. The measurements are calibrated for one-port configuration. Fig. 10 shows the measured and calculated capacitance versus voltage curves of the tunable capacitor with capacitor comb finger lengths ( $L$ ) of 200 and 425  $\mu\text{m}$ , respectively. The measurement data agrees well with the finite element analysis. The tuning range for the 200 and 425  $\mu\text{m}$  finger lengths are 1680% and 3000%, respectively. This is much higher than our previous device (320%) that was built on a 10- $\mu\text{m}$ -thick SOI [13]. The 200- $\mu\text{m}$  comb fingers yield a maximum capacitance of 3.4 pF and a minimum capacitance of 0.2 pF. The longer (425  $\mu\text{m}$ ) comb fingers increase the maximum capacitance to 8.6 pF with a minimum value at 0.27 pF. The increase in the operating voltage in the longer comb device is due to the wider springs employed to increase stability.

The  $S_{11}$  parameter of the 3000% tunable device is shown in Fig. 11. The frequency sweep ranges from 45 MHz to 5 GHz. The quality factor  $Q$  is calculated from either the impedance  $Z$  or  $S_{11}$  value

$$Q = -\frac{\text{Im}(Z)}{\text{Re}(Z)} = \frac{2\text{Im}(S_{11})}{1 - |S_{11}|^2}. \quad (6)$$

Fig. 12 shows that the maximum attainable quality factor for 0.3 pF is 273 at 1 GHz. At lower frequencies and/or smaller

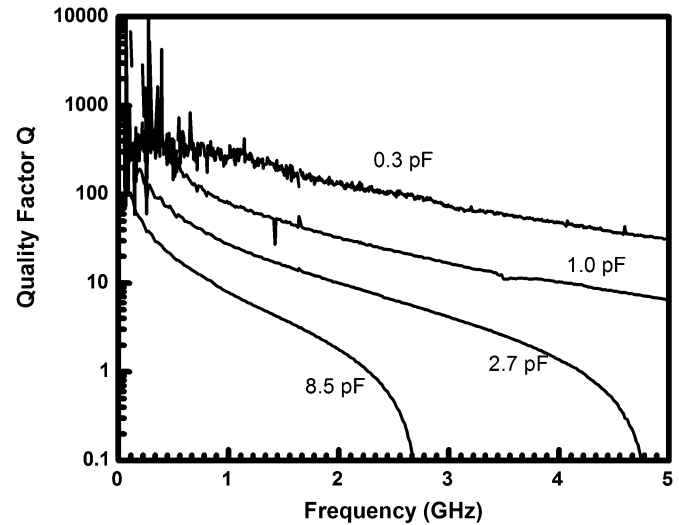


Fig. 12. Quality factor  $Q$  at 8.6 to 0.3 pF from 45 MHz to 5 GHz.

capacitance values and with the  $S_{11}$  being very close to 1, any perturbation or noise from the network analyzer greatly affects the calculated value of  $Q$ . Fig. 12 clearly shows that the plots for smaller capacitances exhibit more noise especially at lower frequencies.  $Q$  can be further improved by increasing the metal thickness. Ultimately having all-metal finger electrodes would be the optimum design for large  $Q$  values. Our results can be compared to the performances of previous MEMS varactors in Table I. The devices operates reliably during our measurement period, however, long-term reliability, being strongly correlated with packaging technology, needs to be investigated and is beyond the scope of this paper.

## V. CONCLUSION

This paper has proposed and reported a successful fabrication of a novel MEMS tunable capacitor with AVC actuators. We have achieved a 3000% continuous tuning range from 0.27 pF to 8.6 pF. We believe the tuning range is the highest ever reported.

TABLE I  
COMPARISON OF THE PERFORMANCES FROM DIFFERENT MEMS VARACTOR APPROACHES

Reference	Voltage	Q (@ Hz)	Capacitance	TR
Gap-closing microbridge [5]	5.5 V	60 (1 GHz)	2 pF	16%
Electro-thermal varactor [2]	< 5 V; 3mA	1050 (1 GHz)	0.5–3.5 pF	100%
CMOS varactor [4]	5 V	23 (1 GHz)	1.4–1.9 pF	35%
Comb drive/parallel plate [10]	20 V	n/a	2.0–8.46 pF	400%
Separated gap-closing [11]	< 77 V	n/a	0.94–5.5 pF	600%
Differential gap-closing [8]	17.2 V	n/a	0.48–0.73 pF	69.8%
Dielectric displacement [1]	20 V	290 (1 GHz)	1.15–1.6 pF	40%
Linear comb drives [12]	8 V	36 (2 GHz)	1.4–11.9 pF	740%
This work (AVC)	40 V	273 (1 GHz)	0.27–8.6 pF	3000%

The quality factor is 273 at 1 GHz for the minimum capacitance of 0.3 pF. Our AVC MEMS varactor shows great promise as next generation phase shifters and filters for microwave systems.

#### ACKNOWLEDGMENT

The authors would like to thank Drs. B. Loo, J. Shaffner, D. Sivenpiper, and G. Tagonan of HRL Laboratories for their valuable discussions. They would especially like to thank S. Mathai, I.-H. Lin, and S. Murthy of the University of California (UCLA), Los Angeles, for their assistance in the microwave measurements.

#### REFERENCES

- [1] J. B. Yoon and C. T. C. Nguyen, "A high-Q tunable mechanical capacitor with moving dielectric for RF applications," in *Proc. International Electron Devices Meeting 2000*, Piscataway, NJ, 2000, pp. 489–492.
- [2] K. F. Harsh, B. Su, W. Zhang, V. M. Bright, and Y. C. Lee, "The realization and design considerations of a flip-chip integrated MEMS tunable capacitor," *Sens. Actuators, Phys. A*, vol. A80, no. 2, pp. 108–118, 1993.
- [3] J. Y. Park, Y. J. Yee, H. J. Nam, and J. U. Bu, "Micromachined RF MEMS tunable capacitors using piezoelectric actuators," in *Proc. Microwave Symposium Digest*, vol. 3, 2001, pp. 2111–2114.
- [4] A. Dec and K. Suyama, "Microwave MEMS-based voltage-controlled oscillators," *IEEE Trans. Microwave Theory Techn.*, vol. 11, pp. 1943–1949, Nov. 2000.
- [5] D. Young and B. E. Boser, "A micromachined-based RF low-noise voltage-controlled oscillator," in *Proc. Custom Integrated Circuit Conference*, 1997, pp. 431–434.
- [6] C. Goldsmith, A. Malczewski, Z. Yao, S. Chen, J. Ehmke, and D. Hinzl, "RF MEMS variable capacitors for tuning filters," *Int. J. RF Microwave Computer-Aided Eng.*, vol. 9, no. 4, pp. 362–374, July 1999.
- [7] J. B. Rizk and G. M. Rebeiz, "Digital-type RF MEMS switch capacitors," in *Proc. IEEE MTT-S International Microwave Symposium*, vol. 2, June 2002, pp. 1217–1220.
- [8] J. Zou, C. Liu, J. Schutt-Aine, J. Chen, and S. M. Kang, "Development of a wide tuning range MEMS tunable capacitor for wireless communication systems," in *Proc. International Electron Devices Meeting 2000*, pp. 403–406.
- [9] A. Dec and K. Suyama, "Micromachined electro-mechanically tunable capacitors and their applications to RF IC's," *IEEE Trans. Microwave Theory Techn.*, vol. 46, no. 12, pp. 2587–2596, Dec. 1998.
- [10] Z. Li and N. C. Tien, "A high tuning-ratio silicon-micromachined variable capacitor with low driving voltage," in *Proc. Solid-State Sensor and Actuator Workshop*, Hilton Head Island, SC, June 2–6, 2002, pp. 239–242.
- [11] Z. Xiao, W. Peng, R. F. Woffenbittel, and K. R. Farmer, "Micromachined variable capacitor with wide tuning range," in *Proc. Solid-State Sensor and Actuator Workshop*, Hilton Head Island, SC, June 2–6, 2002, pp. 346–349.
- [12] R. Borwick, P. Stupar, J. DeNatale, R. Anderson, C. Tsai, and K. Garrett, "A high Q, large tuning range, tunable capacitor for RF applications," in *Proc. MEMS 2002*, Las Vegas, NV, pp. 669–672.
- [13] H. Nguyen, D. Hah, P. Patterson, R. Chao, W. Piyawattanametha, and M. C. Wu M. C., "A novel MEMS tunable capacitor based on angular vertical comb drive actuators," in *Proc. Solid-State Sensor, Actuator and Microsystems Workshop*, Hilton Head Island, SC, June 2002, pp. 277–280.
- [14] [Online]. Available: <http://www.surplussales.com/Variables/Differentials/DiffCap1.html>
- [15] P. Patterson, D. Hah, H. Chang, H. Toshiyoshi, and M. C. Wu, "An angular vertical comb drive actuator for scanning micromirrors," in *Proc. 2001 International Conference on Optical MEMS*, Okinawa, Japan, p. 25. add complete page number.
- [16] D. Hah, H. Toshiyoshi, and M. C. Wu, "Design of electrostatic actuators for MOEMS applications," in *Proc. Design, Test, Integration, and Packaging of MEMS/MOEMS (DTIP 2002)*, Cannes-Mundelein, France, May 6–8, 2002. add page numbers.
- [17] O. Tsuboi, Y. Mizuno, N. Koma, H. Soneda, H. Okuda, S. Ueda, I. Sawaki, and F. Yamagishi, "A rotational comb-driven micromirror with a large deflection angle and low drive voltage," in *Proc. Micro Electro Mechanical Systems 2002*, Las Vegas, NV, pp. 532–535.
- [18] P. W. Green, R. R. A. Syms, and E. M. Yeatman, "Demonstration of three-dimensional microstructure self-assembly," *J. Microelectromech. Syst.*, vol. 4, pp. 170–176, Dec. 1995.
- [19] R. R. A. Syms, "Surface tension powered self-assembly of 3-D micro-optomechanical structures," *J. Microelectromech. Syst.*, vol. 8, pp. 448–455, Dec. 1999.
- [20] B. McCarthy, V. M. Bright, and J. Neff, "A solder self-assembled large angular displacement torisoidal micromirror array," in *Proc. Micro Electro Mechanical Systems* Las Vegas, NV, 2002, pp. 499–502.
- [21] R. A. A. Syms, C. Gormley, and S. Blackstone, "Improving yield, accuracy, and complexity in surface tension self-assembled MOEMS," *Sens. Actuators*, vol. A88, no. 3, pp. 273–283, Mar. 2001.
- [22] A. Tuantranont, V. M. Bright, J. Zhang, W. Zhang, J. A. Neff, and Y. C. Lee, "Optical beam steering using MEMS-controllable microlens array," in *Proc. Solid-State Sensor and Actuator Workshop*, Hilton Head Island, SC, June 4–8, 2000, pp. 363–372.



**Hung D. Nguyen** (S'98) received the B.S. degree in physics and the M.S. degree in electrical engineering at the University of California, Los Angeles (UCLA) in 1998 and 2003, respectively. He is currently pursuing the Ph.D. degree in electrical engineering at UCLA.

His research is mainly in optical MEMS (MOEMS) and RF MEMS. He is a recipient of the Intel Foundation Fellowship for 2004.



**Dooyoung Hah** received the M.S. and Ph.D. degrees in electrical engineering from the Korea Advanced Institute of Science and Technology (KAIST), Korea, in 1996 and 2000, respectively. His Ph.D. dissertation topic was RF MEMS switch.

From 2000 to 2001, he was a Postdoctoral Research Engineer at the University of California, Los Angeles. In 2002, he joined the Electronics and Telecommunications Research Institute (ETRI), Korea as a Senior Member of Engineering Staff. His research interests include MOEMS, RF MEMS, and

microactuators.

Dr. Hah was the third place winner at the student paper competition at 2000 IEEE MTT-S.

**Pamela R. Patterson** (M'00) received the B.S. degree (*cum laude*) from the University of Cincinnati, OH, and the M.S. degree and Ph.D. (2003) degree in electrical engineering from the University of California, Los Angeles (UCLA), completing the dissertation year as recipient of an Intel foundation fellowship.

She has held senior engineering positions at TRW, Varian, and at UCLA, where she helped to establish the Nanoelectronics Research Laboratory from 1994 to 2003. She is currently a research staff member at HRL Laboratories, LLC, Malibu, CA, conducting research on heterogeneous integration of semiconductor materials. Her research interests are in the area of microfabrication process design and technology and she has authored or coauthored 14 conference papers, including three invited papers, and contributed a book chapter (coauthored with Dr. M. Wu) in this field as applied to optical MEMS devices.

Dr. Patterson is a Member of Eta Kappa Nu, AAAS, and AVS.

**Rumin Chao**, photograph and biography not available at the time of publication.

**Wibool Piyawattanametha**, photograph and biography not available at the time of publication.

**Erwin K. Lau** received the B.S. and M.Eng. degrees in electrical engineering from Massachusetts Institute of Technology, Cambridge, in 2000. His Ph.D. research is on semiconductor lasers and RF photonics.



**Ming C. Wu** (S'82–M'83–SM'00–F'02) received the B.S. degree in electrical engineering from National Taiwan University, Taiwan, in 1983 and the M.S. and Ph.D. degrees in electrical engineering and computer sciences from the University of California, Berkeley, in 1985 and 1988, respectively.

From 1988 to 1992, he was a Member of Technical Staff at AT&T Bell Laboratories, Murray Hill. In 1993, he joined the faculty of Electrical Engineering Department of the University of California at Los Angeles (UCLA), where he is currently Professor.

He is also Director of UCLA's Nanoelectronics Research Center, and Vice Chair for Industrial Relations. His current research interests include micro-electromechanical systems (MEMS), optical MEMS (MOEMS), biophotonics, microwave photonics, and high-speed optoelectronics. He has published over 360 papers, contributed four book chapters, and holds 11 U.S. patents.

Dr. Wu was the founding Co-Chair for IEEE LEOS Summer Topical Meeting on Optical MEMS in 1996. The meeting has now evolved into IEEE LEOS International Conference on Optical MEMS that rotates among Europe, Asia, and the United States. He has also served in program committees of many other conferences, including optical fiber communications (OFC), conference on lasers and electrooptics (CLEO), IEEE Conference on Micro Electro Mechanical Systems (MEMS), LEOS Annual Meetings (LEOS), International Electron Device Meeting (IEDM), Device Research Conference (DRC), International Solid-State Circuit Conference (ISSCC), and Microwave Photonics (MWP) Conferences. He is a David and Lucile Packard Foundation Fellow (1992–1997).